Chemical Science

ROYAL SOCIETY OF CHEMISTRY

EDGE ARTICLE

View Article Online
View Journal | View Issue

Cite this: *Chem. Sci.*, 2023, **14**, 2624

All publication charges for this article have been paid for by the Royal Society of Chemistry

Choose your leaving group: selective photodeprotection in a mixture of *p*HP-caged compounds by VIPER excitation†

Luuk J. G. W. van Wilderen, ‡[a] Daniela Kern-Michler, ‡[a] Carsten Neumann,‡[a] Matiss Reinfelds, ‡[b] Jan von Cosel,[c] Maximiliane Horz,[c] Irene Burghardt, [c] Alexander Heckel [b] and Jens Bredenbeck *[a]

Photocages are light-triggerable molecular moieties that can locally release a pre-determined leaving group (LG). Finding a suitable photocage for a particular application may be challenging, as the choice may be limited by for instance the optical or physicochemical properties of the system. Using more than one photocage to release different LGs in a reaction mixture may even be more difficult. In this work an experimental strategy is presented that allows us to hand-pick the release of different LGs, and to do so in any order. This is achieved by using isotopologue photocage–LG mixtures in combination with ultrafast VIbrationally Promoted Electronic Resonance (VIPER) excitation. The latter provides the required molecular selectivity simply by tuning the wavenumber of the used IR pulses to the resonance of a specific photocage isotopologue, as is demonstrated here for the *para*-hydroxyphenacyl (*p*HP) photocage. For spectroscopic convenience, we use isotopologues of the infrared (IR) spectroscopic marker –SCN as different LGs. Especially for applications where fast LG release is required, *p*HP is found to be an excellent candidate, as free LG formation is observed to occur with a 10 ps lifetime. The devised strategy may open up new complex uncaging applications, where multiple LGs can be formed locally on a short time scale and in any sequence.

Received 11th November 2022
Accepted 7th February 2023

DOI: 10.1039/d2sc06259c

rsc.li/chemical-science

Introduction

Photocages are powerful tools to locally release a predetermined molecular compound by light at a specific point in time. Choosing the right photocage for a particular application requires a biological, chemical and/or physical compatibility of the photocage, the photoreaction, and the system where it is employed in. Continuous efforts are put into novel uncaging strategies, ranging from the introduction of multiple LGs into a single photocage[1,2] to pushing the photocage's optical properties to allow near-IR excitation with one[3,4] or two photons.[5–7] Another optical method is VIbrationally Promoted Electronic Resonance (VIPER) spectroscopy, which can be used to perform sub-ensemble selective photochemistry.[8] Such an ensemble can for instance consist of an isotopologue mixture of photocages.[9] With VIPER, we demonstrated selective excitation of isotopomers of a coumarin photocage.[9] In this work, we build upon these experiments and for the first time demonstrate the release of selected leaving groups (LGs).

We focus here on the small *para*-hydroxyphenacyl (*p*HP) photocage. As LGs different isotopologues of the –SCN moiety (see Scheme 1) are chosen for spectroscopic convenience, allowing us to directly detect the successful release of the LG of choice in the IR. The spectroscopic selection is based on (tunable) vibrational excitation, after which the selected photocage is electronically excited and its photochemistry is subsequently initiated. In the gas phase, related experiments (with IR excitation, subsequent UV/VIS excitation and *e.g.* ion or fluorescence detection) have been used to investigate photochemistry starting from defined and sometimes highly excited vibrational states,[10,11] or to obtain the IR spectra of molecules in molecular beams.[12]

*p*HP is a photolabile protection group (PPG) well known for its high quantum yield and clean photochemistry in aqueous solutions.[13–18] The irreversible uncaging mechanism (Scheme 1) after excitation to the S_1 state in water consists of the formation of a triplet intermediate, the deprotonation of the phenolic head group (not shown), and consecutive Favorskii bond rearrangements. The latter leads to *para*-hydroxyphenyl acetate (*p*HPA) in

[a]*Johann Wolfgang Goethe-University, Institute of Biophysics, Max-von-Laue-Str. 1, 60438 Frankfurt am Main, Germany. E-mail: bredenbeck@biophysik.uni-frankfurt.de*
[b]*Johann Wolfgang Goethe-University, Institute of Organic Chemistry and Chemical Biology, Max-von-Laue-Str. 7, 60438 Frankfurt am Main, Germany*
[c]*Johann Wolfgang Goethe-University, Institute of Physical and Theoretical Chemistry, Max-von-Laue-Str. 7, 60438 Frankfurt am Main, Germany*

† Electronic supplementary information (ESI) available: The ESI shows DFT computations of *p*HP–SCN, an extended uncaging reaction mechanism, global fitting results for different D_2O : MeCN ratios, VIPER computations and steady-state spectra of the isotopologues. See DOI: https://doi.org/10.1039/d2sc06259c

‡ These authors contributed equally.

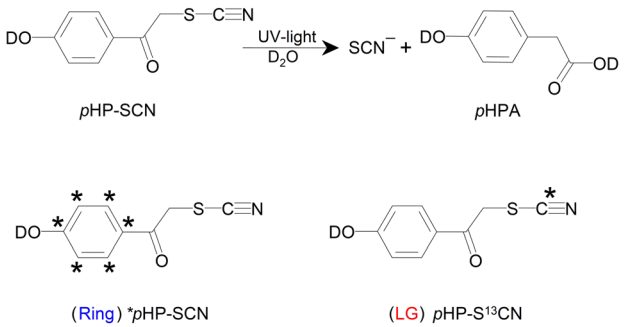

Scheme 1 Simplified reaction scheme for the photocleavage of *p*HP–SCN (top row). Two separate isotopologues are prepared, *i.e.* the ring-labelled 'Ring' compound and the LG-labelled 'LG' compound (bottom row). The stars denote the inserted ^{13}C positions. Depending on the starting compound, photocleavage leads to the release of the isotope labelled or unlabelled LG.

the presence of water. The LG is already cleaved during the deprotonation step, but its release has not directly been observed so far in time-resolved spectroscopy.[17–26] *p*HP has been promoted as an alternative for the widely used *o*-nitrobenzyl derivatives. In addition to the much cleaner photoreaction that does not produce toxic byproducts, *p*HP cleavage is very fast (orders of magnitude faster) and therefore suitable for kinetic studies.[27] The photoproduct has a blue-shifted absorption with respect to the starting material and is therefore not competing for excitation photons. The uncaging quantum yield is not strongly LG-dependent but is found to generally increase with decreasing pK_a values.[27]

The applications of *p*HP as a PPG encompass neurobiology,[17,28–35] enzyme catalysis, where fast uncaging is essential,[17,27,34,36–38] biochemistry, such as in drug-delivery or the release of nucleobases, amines and NAD^+,[39–42] supramolecular chemistry,[43] controlled etching of surfaces,[44] and tissue engineering *via* hydrogel foams that can be used as scaffolds.[45] There are currently ongoing efforts to increase the quantum yield of release of phenolic LGs such as the amino acid tyrosine.[46] Extending the already vast application range for *p*HP further, it is shown here that even multiple simultaneously present *p*HP–SCN isotopologues can be used, which, in conjunction with VIPER, makes product release on demand from a desired *p*HP–LG combination feasible. SCN is chosen as the LG for demonstration because it is easily identifiable in the IR. First the uncaging of each individual *p*HP–SCN isotopologue is presented, after which the species-selective VIPER pulse sequence is applied to their mixture.

Materials and methods

Synthesis

The compound with a ^{13}C label in each position of the aromatic ring is prepared in a Friedel–Crafts acylation of ^{13}C-labelled phenol with 2-bromoacetyl chloride,[47] followed by reaction with NH_4SCN. The same reaction is used for the preparation of the derivative with a ^{13}C label in the LG, using $KS^{13}CN$ instead. For synthesis and characterization details, see the ESI and Fig. S1–S7.† NMR, high resolution mass spectrometry (HRMS) and IR spectroscopy confirmed the isotope incorporation. For the laser experiments, the samples are dissolved in D_2O (Eurisotop) and acetonitrile (MeCN; Sigma-Aldrich), and dried with a molecular sieve before use.

Spectroscopy

FTIR spectroscopy is performed on a Bruker Tensor 27. Samples are circulated in a closed cycle incorporating two flow cells[48] with CaF_2 windows. One cell is positioned inside the FTIR spectrometer. Illumination is done outside the FTIR in the second flow cell using a UV-C lamp (Brita) emitting at 253 nm. The spectra are corrected for solvent absorption.

UV/VIS absorption spectra are collected with a JASCO V-670 spectrometer in a flow cell. The recorded FTIR and UV/VIS spectra with and without illumination are shown in Fig. S8.† In addition, the FTIR spectra of several structurally similar reference compounds are shown in Fig. S9.†

Ultrafast measurements are done using a Ti:sapphire regenerative amplifier (Spitfire XP, Spectra Physics) producing 3 mJ of 100 fs pulses at 800 nm and at 1 kHz. The Spitfire XP pumped three home-built OPAs. Signal and idler pulses of two OPAs generated in a BBO crystal are mixed in $AgGaS_2$ to obtain mid-IR pump and probe pulses *via* difference frequency generation. The probe beam is split into two beams for referenced detection on a 2 × 32 pixel MCT detector (Infrared Associates) behind a spectrometer (Triax 180, Horiba) with a 150 l mm^{-1} grating. The focus size of both probe and reference IR beams in the sample is about 80 μm × 80 μm.

For resonant UV pump–IR probe measurements, the UV is generated *via* tripling of the Spitfire's fundamental to generate 266 nm (focus size 90 μm × 120 μm; 2 μJ per pulse; a few hundred femtoseconds long) and mechanically delayed and chopped at 500 Hz (Fig. S14†). The relative polarization is set to the magic angle with respect to the probe beam. The sample in the flow cell is continuously pumped around (1 ml total volume) to exchange the sample between laser shots and mechanically moved up and down to prevent the increase of scatter form the windows over time.

The narrowband IR pump pulses for the VIPER measurements are generated using a Fabry–Pérot interferometer (FWHM 22 cm^{-1}; ~0.2 μJ per pulse; focus size at the sample 110 μm × 120 μm) and mechanically delayed and chopped at 250 Hz. The overall chopping scheme is as described earlier.[8] The flow cell is continuously translated as was done for the pump–probe experiments. Off-resonant UV pulses for VIPER excitation at 320 nm are generated by sum-frequency generation of the doubled fundamental and signal beams (UV focus size 145 μm × 125 μm). The UV pump (3.3 μJ per pulse) is blocked when the delay lines are moving to avoid unnecessary sample illumination. The polarizations of the beams are optimized for the VIPER signal size and set to 20° between the IR and UV pump pulses. The IR probe pulses are oriented parallel with respect to the UV pump pulse. The delay between the IR pump and UV pump is set to 1 ps to avoid pulse overlap. For all laser measurements the signal at −20 ps is subtracted as the background.

Computations

The harmonic vibrational frequencies of *p*HP–SCN are obtained after optimization of the ground state geometry using analytical first and second derivatives and employing the PBE0 functional[49] and Def2-TZVP basis set[50] as implemented in Gaussian 16 Rev. B.01.[51] The solvent effects of MeCN have been accounted for by the Conductor-like Polarizable Continuum Model (CPCM). The explicit influence of the vibrational pre-excitation of a predetermined normal mode on the UV/VIS spectrum has been investigated *via* the efficient computation of vibrationally resolved absorption spectra with FCClasses,[52,53] as proposed in a previous study.[54] Necessary ground and singlet excited state calculations were obtained using the PBE0 functional and Def2-TZVP basis set. Both IR and UV/VIS spectra are convoluted with either Lorentzian or Gaussian envelope functions, respectively, to match their experimental counterpart.

Results

*p*HP–SCN cleavage

The photocleavage of *p*HP–SCN produces a free SCN^- ion and the main photoproduct *p*HPA as shown in Scheme 1. Unilluminated *p*HP–SCN shows three distinct bands at 1515 cm^{-1}, 1575 cm^{-1} and 1602 cm^{-1} in the IR (Fig. 1A), which are all assigned to ring modes using DFT computations (see Fig. S10†). The band at 1669 cm^{-1} is assigned to mainly νC=O and the band at 2160 cm^{-1} to νCN of the covalently bound SCN.

Next, UV/VIS pump–IR probe data of *p*HP–SCN were collected in order to monitor the ultrafast cleavage reaction. To our knowledge, ultrafast release of the LG is directly observed for the first time. In Fig. 1 we show the global analysis (GA) of the data in a solvent mixture of D_2O : MeCN (1 : 8), as water is required for the photoreaction. The resulting species-associated difference spectra (SADS) in Fig. 1B (see also Fig. S11B,† where each spectrum is plotted with an offset) show that the black spectrum decays with 5.5 ps to become the red spectrum. Its lifetime is consistent with intersystem crossing (ISC) from the singlet S_1 to the triplet T_1 state and will be referred to as τ_{isc}.[20] Prominent spectral changes on this timescale are the disappearing positive feature from about 1520 cm^{-1} to 1565 cm^{-1} (see number 1 in Fig. 1B), assigned to a singlet ESA feature of one or more ring modes, and the upshift of the bound SCN's ESA around 2140 cm^{-1}, assigned to vibrational cooling (number 2). The νCN mode of the free SCN ion absorbs around 2060 cm^{-1} and appears on a tens of ps timescale with $\tau_{release}$ (number 3), implying that the LG detaches from T_1. The small amplitude at 2060 cm^{-1} in the red and black SADS shows the onset of the formation of free SCN ions already within a few ps.

The τ_{rec} = 19.8 ps lifetime (from blue to bright green) is associated with a disappearance of the ESA feature at 2140 cm^{-1} (number 4) and a small recovery of the bleach at 2160 cm^{-1}, both pointing to ground state recovery of a fraction of the photoexcited molecules (with the LG still attached). The recovery is consistent with a decrease of the main bleach at 1602 cm^{-1} on the same time scale (number 5).

The next time constant ($\tau_{photoprod}$ = 556 ps) is associated with *p*HPA photoproduct formation, as evident from the induced

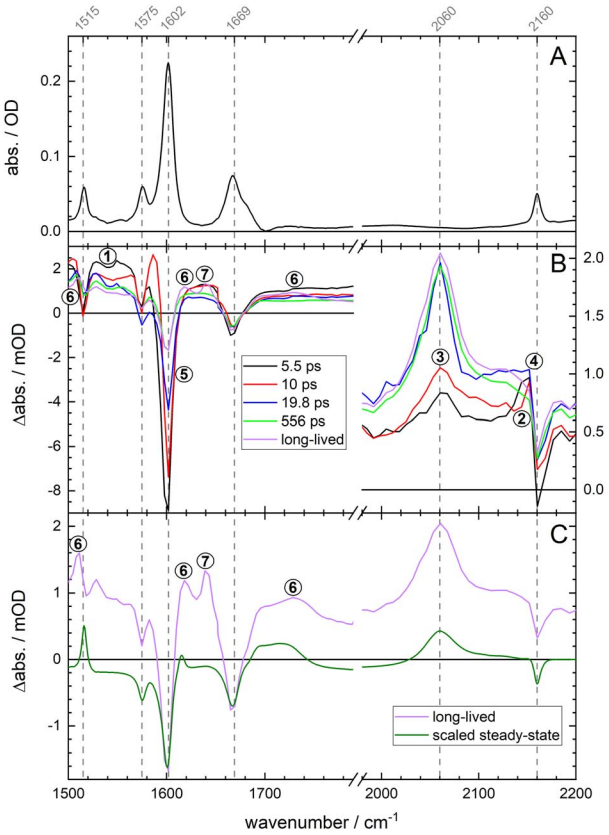

Fig. 1 Panel (A) shows the steady-state FTIR absorption spectrum of an unilluminated sample (about 30 mM in a CaF_2 cell with a 50 μm Teflon spacer). Panel (B) shows the species-associated absorption difference spectra (SADS) of *p*HP–SCN after 320 nm excitation (100 mM; 50 μm spacer). The legend shows the associated time constants. Two additional components are needed to fit the coherent artefact around time zero (not shown). The signals in the SCN region have a different ordinate (shown to the right of the axis). Panel (C) compares the slowest SADS of panel (B) to a scaled FTIR light-induced difference spectrum (30 mM; 100 μm spacer). Fig. S11† reproduces the SADS with an added offset to the spectra below 1800 cm^{-1} for improved readability. Fig. S12 and S13† show raw spectra and time traces with fits and residuals. All data are collected using 1 : 8 D_2O : MeCN as solvent. Data using 1 : 1 D_2O : MeCN and their associated fits are shown in Fig. S14–S16.†

absorptions around 1720 cm^{-1}, 1615 cm^{-1} and 1510 cm^{-1} in the purple spectrum (see the numbers 6 in Fig. 1B and C), which all show striking similarities with the absorption spectrum of *p*HPA (see Fig. S8C†). There is an additional induced feature around 1640 cm^{-1} (number 7) that might belong to an intermediate. The position would indicate that it is related to a carbonyl absorption, although it could also be an up-shifted ring mode. The bleaches in the long-lived SADS resemble those of the steady-state difference spectrum (see Fig. 1C) and indicate irreversible, successful photochemistry. A coarse estimate of the uncaging yield is about 20% (based on the relative signal amplitudes at early and late times at 1602 cm^{-1}).

Our data are consistent with the literature on other *p*HP photocages,[24,55] for instance that reported for *p*HP–diethyl phosphate (in H_2O).[24] For that compound τ_{isc} = 4 ps and τ_{T_1} =

60 ps are found, with LG cleavage occurring during triplet state formation. Although we cannot unambiguously assign the S_1 and the T_1 states in our data, the release of the SCN ion obviously occurs on a tens of ps time scale. The subsequent rate $\tau_{photoprod}$ found here for *p*HPA product formation is also consistent with the literature and depends on the LG and water content (from μs in dry solvents down to about $\tau_{photoprod} = 60$ ps for the mentioned phosphate compound).[24]

*p*HP–SCN isotopologues

Having established here that the release of the LG is directly spectroscopically observable, two *p*HP–SCN isotopologues have been synthesized. One contains a single ^{13}C isotope in the LG (*p*HP–S^{13}CN), and the other has all ring carbons replaced (**p*HP–SCN). The isotopologues correspond to the LG and R compounds, respectively, as depicted in Scheme 1. The purpose of the LG-isotopologue is to down-shift the *ν*CN mode with respect to the ring-labelled compound, making an unambiguous distinction of the compounds (as well as their released ions) that underwent photochemistry possible. The spectral shifts of the SCN features are seen in the light-minus-dark difference spectra in Fig. 2A, where each compound is measured separately. As the UV/VIS absorption spectra of the two isotopologues are indistinguishable (see Fig. S17†), continuous illumination of a 50 : 50 isotopologue mixture (at 253 nm) leads to the superposition of the individual light-induced difference spectra as shown in Fig. 2B. The same spectral changes are visible after resonant pulsed laser excitation at 320 nm and at a delay of 100 ps (Fig. 2C). Again, the UV wavelength is equally resonant with either isotopologue and leads to indiscriminate excitation of the two co-existing compounds in the mixture (Fig. 2D). In contrast, it will be shown below that the application of the VIPER pulse sequence allows us to perform and monitor isotopologue-selective photochemistry, using the UV pulse in combination with a preceding tunable narrowband IR pulse.

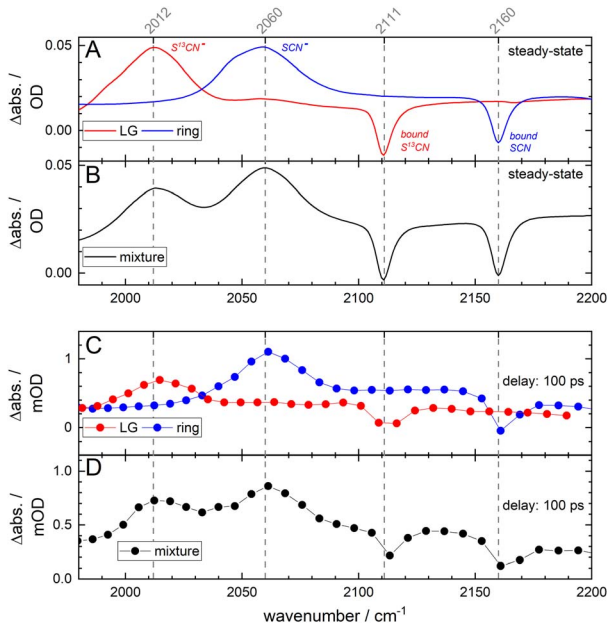

Fig. 2 Steady-state and time-resolved difference spectra of the individual compounds as well as that of a 50 : 50 mixture. All samples are dissolved in 1 : 8 D_2O : MeCN (100 mM; 50 μm spacer). Panel (A) shows the light-minus-dark FTIR difference spectra for the single LG- and ring-labelled compounds, and panel (B) that of the 50 : 50 mixture. Panel (A) also shows the band assignments. Panels (C) and (D) show the time-resolved difference spectra after a pump–probe time delay of 100 ps (after 320 nm excitation).

VIPER uncaging

One crucial advantage of IR over UV/VIS spectroscopy is that the absorption spectra have narrower line shapes. Different compounds and mixtures are therefore easier to identify as spectral overlap is generally less severe. The VIPER pulse sequence utilizes the inherently higher spectral and structural selectivity in the IR. In the case of isotopologues, the associated vibrational modes will be modulated by the different isotope compositions, making it possible to vibrationally excite either compound with a narrowband IR pulse. The applied VIPER excitation actually consists of two pulses, *i.e.* a tunable IR pulse, followed by a UV/VIS pulse. If the energy of the IR and UV/VIS photons combined is sufficient to reach S_1, photochemistry can be induced. Potential contributions from direct UV/VIS excitation are eliminated by means of a chopping scheme, as any underlying signals (arising from for instance IR-pump IR-probe and UV/VIS-pump IR-probe sequences) are monitored and corrected for.[8] As can be seen in Fig. S17,† *p*HP–SCN's main absorption lies around 285 nm, while for the VIPER 2D-IR data shown in Fig. 3 the UV pulse is set to a not fully resonant wavelength of 320 nm. The latter UV pump wavelength was chosen as it produced the largest observed VIPER signals on the red side of the absorption spectrum, in agreement with the theoretically predicted IR-induced shift of the UV spectrum of the S_1 state (Fig. S18†).

Now, we apply VIPER to a mixture of codissolved isotopologues, by first tuning the IR pulse to be absorbed by (the ring modes of) the ring-labelled compound, as depicted by the blue Lorentzian pulse above Fig. 3A. The ring modes are chosen here, as they are theoretically predicted to show the largest VIPER effect[54] for either isotopologue (see Fig. S18†). After the IR pump pulse, the UV pump pulse arrives at $t_1 = 1$ ps (see Fig. 3C), followed by a broadband IR probe pulse after $t_2 = 100$ ps. The first delay t_1 is chosen to be longer than the duration of the IR pump pulse (~0.7 ps), and the second delay t_2 to be at a delay much longer than $\tau_{release} = 10$ ps. The VIPER spectra in the rightmost panel of Fig. 3C clearly show that vibrational excitation of the blue ring-labelled compound only produces SCN features that are associated with the release of the unlabelled LG. Tuning the IR pulse now to the ring modes of the LG-labelled compound (schematically depicted in Fig. 3C by the vertical color-coded arrows in the schematic energy level diagram), uncaging is only observed from the LG-labelled compound (red). It is thus possible to select which LG will be released, even when structurally and spectroscopically similar molecules are present. In other words, in molecular mixtures where selective UV/VIS excitation is not possible, VIPER may still be able to activate one particular photoreaction or release the LG of choice. As the absolute size of

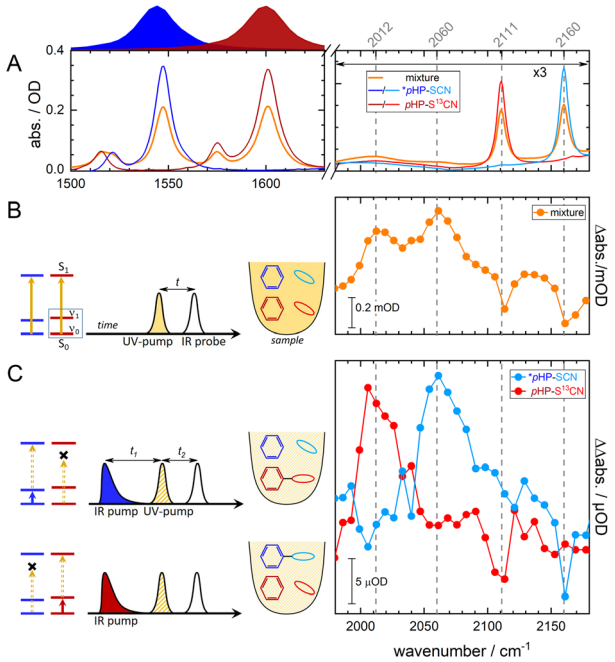

Fig. 3 Ultrafast VIPER uncaging of a 50 : 50 mixture of the LG- and ring-isotopologues. The LG isotopologue is depicted using shades of red, the ring-isotopologue by shades of blue, and their mixture of orange. Panel (A) shows the FTIR absorption spectra of the two isolated compounds and of their mixture. The absorption in the SCN spectral region is multiplied by a factor of three. Panel (B) shows that simple resonant UV excitation at 320 nm of the mixture, symbolized by the vertical dark orange line in the schematic energy level scheme, the same-colored sample container and the color-coded chemical structures of the compounds, leads to non-preferential uncaging. The spectrum is collected at a delay of $t = 100$ ps. Panel (C) shows that the application of the VIPER pulse sequence to the same mixture used in panel (B) leads to preferential photochemistry of the desired compound. The approach consists of vibrational pre-excitation of one compound, using a tunable narrowband IR pulse (depicted above panel (A) and as a vertical blue or red arrow in the energy level scheme) that is followed by a second off-resonant 320 nm UV-pump pulse (the dashed vertical arrow in the energy level scheme and the diagonally shaded pulse), promoting the photochemistry of the pre-excited compound. The time delays between the pulses are $t_1 = 1$ ps and $t_2 = 100$ ps. The total *p*HP–SCN concentration of the mixture is 100 mM in 1 : 8 D_2O : MeCN.

the VIPER signals of *p*HP is comparably small, we had to tune the UV pulse to be relatively resonant (320 nm). On the one hand, this increases the VIPER signal (Fig. 3C) above our detection threshold, and on the other hand this increases the direct excitation signal (Fig. 3B), so that the VIPER/direct excitation ratio is 0.05 only. In spectroscopic applications, *e.g.* when monitoring the photochemistry after the selection of a species, the direct excitation itself is not a problem, because its contribution can be subtracted. In applications where purity in a chemical sense matters (*e.g.* when only the VIPER-selected molecules are to be isolated), direct unselective excitation is not desired and can be reduced by means of more off resonant excitation. Other ways to increase the VIPER/direct excitation contrast as well as the absolute size of the VIPER signal is to increase the IR pump energy, as the beam in our spectroscopy setup has an energy of ~200 nJ per pulse only. Light sources that deliver 400 times more pulse energy per wavenumber are already available.[56] A comparison of the kinetics for *p*HP after resonant UV/VIS excitation and VIPER excitation is currently challenging due to the small available VIPER signal sizes, but will be possible with the mentioned improvements in the future. However, even with the current setup we observed VIPER/direct excitation ratios > 20 for another molecule (coumarin 6, not shown) and VIPER signals in the mOD range. The ratio and the absolute VIPER signal size can thus be further optimized by selecting or designing molecules featuring a steep red edge of the UV/VIS spectrum and an optimized VIPER efficiency. A prerequisite of efficient VIPER excitation is that excitation of the IR mode strongly red-shifts the electronic absorption band. Such couplings and their mode dependencies have been predicted and demonstrated experimentally.[54]

Conclusions

PPGs find widespread use in a vast range of applications. Using mixtures of photocage–LG combinations may become problematic if the electronic transitions required for uncaging cannot be addressed independently for each photocage. In that case, it will unavoidably result in indiscriminate and simultaneous release of all LGs. One solution may be to sequentially 'burn away' one population after the other, but this may not always be a viable option. Alternatively, VIPER uncaging can be used, exploiting the isotopologue selectivity in the IR for different PPG–LG combinations. A showcase example is presented in this study, where VIPER is applied to two isotopologues of *p*HP–SCN. It is shown that it is possible to release the desired LG on demand, from a solution of multiple co-existing photocages. This approach can readily be extended to more than two isotopologues if they are designed to have distinguishable IR spectra.

VIPER excitation in general can be further enhanced by using already available stronger IR pump sources,[56] as well as by designing photocages with enhanced VIPER efficiencies. Both of these measures will also improve the VIPER/direct excitation ratio.

The currently limited number of photoconverted molecules may already be characterizable with other methods (*e.g.* mass spectrometry), when a special sample cell is designed for retrieving only the VIPER-illuminated part of the sample. The obtained amount is already sufficient for microscopy applications[57] or for the triggering of reactions in small sample volumes.

Our current study exploits the excitation of IR modes in a spectral region where aqueous solutions also absorb which is of particular importance for biological and biochemical applications. This complication can be overcome by the pumping and probing of IR transitions in a spectral region which has a low water background absorption, by using deuterated solvents which shift the solvent absorption modes away or using thinner samples. For application in aqueous solution, the design of photocages that feature VIPER-active IR modes in spectral regions with lower water absorption (such as nitriles and azides) is another possibility.

Challenges for VIPER excitation are similar to those of other non-linear excitation techniques such as two-photon

uncaging,[58] which is already routinely used in biological settings, and range from a limited number of pump photons, relatively low yields when compared to single photon excitation, raster scanning when larger amounts of sample need to be illuminated, to the need for specialized instrumentation.

The *p*HP–SCN photocage investigated here is especially suitable for time-resolved studies, as LG release is spectroscopically observed to take place with a 10 ps time constant.

By using the example of *p*HP, the ultrafast VIPER pulse sequence is shown to expand currently available uncaging strategies even further, for instance by applying VIPER to mixtures of identical photocages with different LGs. In that case having identified one suitable photocage for a system is already sufficient, and further tedious photocage-screening efforts can be omitted.

Data availability

Data is available from the authors on request.

Author contributions

Conceptualization: L. vW., J. B. (lead); I. B., A. H. (supporting). Data curation: L. vW. (lead); D. K.-M., C. N., J. vC., M. H. (supporting). Formal analysis: L. vW. (lead); D. K.-M., C. N., J. vC., M. R. (supporting). Funding acquisition: I. B., A. H., J. B. (lead); L. vW. (supporting). Investigation: D. K.-M., C. N., J. vC., M. R. (lead); L. vW. (supporting). Methodology: L. vW., J. B. (lead). Project administration: L. vW., J. B. (lead); I. B., A. H. (supporting). Resources: All. Software: L. vW., J. vC., M. H. (equal). Supervision: L. vW., J. B., I. B., A. H. (equal). Validation: D. K.-M., C. N., J. vC., M. H., M. R. (equal). Visualization: L. vW., D. K.-M. (equal). Writing – original draft preparation: L. vW., D. K.-M., C. N. (lead); M. R. (supporting). Writing – review and editing: J. B. (lead), M. R. (supporting).

Conflicts of interest

There are no conflicts to declare.

Acknowledgements

The authors thank the HRZ for computations. Mass spectra were collected by Matthias Brandl of the mass spectrometry service unit of the Institute for Pharmaceutical Chemistry (Goethe University). The authors thank the Deutsche Forschungsgemeinschaft for funding (grant no. 466145756 and RTG 1986 "Complex Scenarios of Light Control"). JB thanks the Alexander von Humboldt Foundation for a Sofja Kovalevskaja award.

References

1 I. Elamri, C. Abdellaoui, J. K. Bains, K. F. Hohmann, S. L. Gande, E. Stirnal, J. Wachtveitl and H. Schwalbe, *J. Am. Chem. Soc.*, 2021, **143**, 10596.
2 H.-M. Hung and T.-S. A. Wang, *ACS Chem. Biol.*, 2022, **17**, 11.
3 T. A. Shell and D. S. Lawrence, *Acc. Chem. Res.*, 2015, **48**, 2866.
4 P. Shrestha, K. C. Dissanayake, E. J. Gehrmann, C. S. Wijesooriya, A. Mukhopadhyay, E. A. Smith and A. H. Winter, *J. Am. Chem. Soc.*, 2020, **142**, 15505.
5 S. Gug, F. Bolze, A. Specht, C. Bourgogne, M. Goeldner and J.-F. Nicoud, *Angew. Chem., Int. Ed.*, 2008, **47**, 9525.
6 A. L. Houk, R. S. Givens and C. G. Elles, *J. Phys. Chem. B*, 2016, **120**, 3178.
7 G. C. R. Ellis-Davies, *Front. Synaptic Neurosci.*, 2018, **10**, 48.
8 L. J. G. W. van Wilderen, A. T. Messmer and J. Bredenbeck, *Angew. Chem., Int. Ed.*, 2014, **53**, 2667.
9 D. Kern-Michler, C. Neumann, N. Mielke, L. J. G. W. van Wilderen, M. Reinfelds, J. von Cosel, F. Santoro, A. Heckel, I. Burghardt and J. Bredenbeck, *J. Am. Chem. Soc.*, 2018, **140**, 926.
10 I. Bar and S. Rosenwaks, *Int. Rev. Phys. Chem.*, 2001, **20**, 711.
11 F. F. Crim, *J. Phys. Chem.*, 1996, **100**, 12725.
12 R. N. Pribble and T. S. Zwier, *Science*, 1994, **265**, 75.
13 R. S. Givens and B. Matuszewski, *J. Am. Chem. Soc.*, 1984, **106**, 6860.
14 R. S. Givens, P. S. Athey, B. Matuszewski, L. W. Kueper, J. Xue and T. Fister, *J. Am. Chem. Soc.*, 1993, **115**, 6001.
15 R. S. Givens and C.-H. Park, *Tetrahedron Lett.*, 1996, **37**, 6259.
16 C.-H. Park and R. S. Givens, *J. Am. Chem. Soc.*, 1997, **119**, 2453.
17 R. S. Givens and J.-I. Lee, *J. Photosci.*, 2003, 37.
18 P. Klán, T. Šolomek, C. G. Bochet, A. Blanc, R. Givens, M. Rubina, V. Popik, A. Kostikov and J. Wirz, *Chem. Rev.*, 2013, **113**, 119.
19 K. Zhang, J. E. T. Corrie, V. R. N. Munasinghe and P. Wan, *J. Am. Chem. Soc.*, 1999, **121**, 5625.
20 P. G. Conrad, R. S. Givens, B. Hellrung, C. S. Rajesh, M. Ramseier and J. Wirz, *J. Am. Chem. Soc.*, 2000, **122**, 9346.
21 C. Ma, W. S. Chan, W. M. Kwok, P. Zuo and D. L. Phillips, *J. Phys. Chem. B*, 2004, **108**, 9264.
22 C. Ma, P. Zuo, W. M. Kwok, W. S. Chan, J. T. W. Kan, P. H. Toy and D. L. Phillips, *J. Org. Chem.*, 2004, **69**, 6641.
23 C. Ma, W. M. Kwok, W. S. Chan, P. Zuo, J. T. Wai Kan, P. H. Toy and D. L. Phillips, *J. Am. Chem. Soc.*, 2005, **127**, 1463.
24 R. S. Givens, D. Heger, B. Hellrung, Y. Kamdzhilov, M. Mac, P. G. Conrad, E. Cope, J. I. Lee, J. F. Mata-Segreda, R. L. Schowen and J. Wirz, *J. Am. Chem. Soc.*, 2008, **130**, 3307.
25 R. S. Givens, M. Rubina and K. F. Stensrud, *J. Org. Chem.*, 2013, **78**, 1709.
26 V. B. Kammath, T. Šolomek, B. P. Ngoy, D. Heger, P. Klán, M. Rubina and R. S. Givens, *J. Org. Chem.*, 2013, **78**, 1718.
27 R. S. Givens, M. Rubina and J. Wirz, *Photochem. Photobiol. Sci.*, 2012, **11**, 472.
28 R. S. Givens and A. L. Yousef, in *Dynamic Studies in Biology: Phototriggers, Photoswitches and Caged Biomolecules*, 2005, pp. 55–75.
29 R. S. Givens, J. F. Weber, A. H. Jung and C. H. Park, *Methods Enzymol.*, 1998, **291**, 1.
30 A. P. Pelliccioli and J. Wirz, *Photochem. Photobiol. Sci.*, 2002, **1**, 441.

31 K. Kandler, L. C. Katz and J. A. Kauer, *Nat. Neurosci.*, 1998, **1**, 119.
32 R. S. Givens, J. F. W. Weber, P. G. Conrad, G. Orosz, S. L. Donahue and S. A. Thayer, *J. Am. Chem. Soc.*, 2000, **122**, 2687.
33 X. Du, *J. Biol. Chem.*, 2000, **275**, 8492.
34 G. Arabaci, X.-C. Guo, K. D. Beebe, K. M. Coggeshall and D. Pei, *J. Am. Chem. Soc.*, 1999, **121**, 5085.
35 R. S. Givens, A. Jung, C.-H. Park, J. Weber and W. Bartlett, *J. Am. Chem. Soc.*, 1997, **119**, 8369.
36 S. Geibel, A. Barth, S. Amslinger, A. H. Jung, C. Burzik, R. J. Clarke, R. S. Givens and K. Fendler, *Biophys. J.*, 2000, **79**, 1346.
37 X. Du, H. Frei and S. H. Kim, *Biopolymers*, 2001, **62**, 147.
38 C. Chang, T. Fernandez, R. Panchal and H. Bayley, *J. Am. Chem. Soc.*, 1998, **120**, 7661.
39 F. Salahi, V. Purohit, G. Ferraudi, C. Stauffacher, O. Wiest and P. Helquist, *Org. Lett.*, 2018, **20**, 2547.
40 D. Madea, T. Slanina and P. Klán, *Chem. Commun.*, 2016, **52**, 12901.
41 I. Bownik, P. Šebej, J. Literák, D. Heger, Z. Šimek, R. S. Givens and P. Klán, *J. Org. Chem.*, 2015, **80**, 9713.
42 A. Rodrigues-Correia, D. Knapp-Bühle, J. W. Engels and A. Heckel, *Org. Lett.*, 2014, **16**, 5128.
43 P. Jagadesan, J. P. Da Silva, R. S. Givens and V. Ramamurthy, *Org. Lett.*, 2015, **17**, 1276.
44 T. Slanina, P. Šebej, A. Heckel, R. S. Givens and P. Klán, *Org. Lett.*, 2015, **17**, 4814.
45 K. K. Adatia, T. Halbritter, M. Reinfelds, A. Michele, M. Tran, S. Laschat, A. Heckel, G. E. M. Tovar and A. Southan, *ChemPhotoChem*, 2020, **4**, 207.
46 T. Field, J. Peterson, C. Ma, P. Jagadesan, J. P. Da Silva, M. Rubina, V. Ramamurthy and R. S. Givens, *Photochem. Photobiol. Sci.*, 2020, **19**, 1364.
47 R. Murashige, Y. Hayashi, S. Ohmori, A. Torii, Y. Aizu, Y. Muto, Y. Murai, Y. Oda and M. Hashimoto, *Tetrahedron*, 2011, **67**, 641.
48 J. Bredenbeck and P. Hamm, *Rev. Sci. Instrum.*, 2003, **74**, 3188.
49 C. Adamo and V. Barone, *J. Chem. Phys.*, 1999, **110**, 6158.
50 F. Weigend and R. Ahlrichs, *Phys. Chem. Chem. Phys.*, 2005, **7**, 3297.
51 M. Frisch, G. Trucks, H. Schlegel, G. Scuseria, M. Robb, J. Cheeseman, G. Scalmani, V. Barone, G. Petersson, H. Nakatsuji, X. Li, M. Caricato, A. Marenich, J. Bloino, B. Janesko, R. Gomperts, B. Mennucci, H. Hratchian, J. Ortiz, A. Izmaylov, J. Sonnenberg, D. Williams-Young, F. Ding, F. Lipparini, F. Egidi, J. Goings, B. Peng, A. Petrone, T. Henderson, D. Ranasinghe, V. Zakrzewski, J. Gao, N. Rega, G. Zheng, W. Liang, M. Hada, M. Ehara, K. Toyota, R. Fukuda, J. Hasegawa, M. Ishida, T. Nakajima, Y. Honda, O. Kitao, H. Nakai, T. Vreven, K. Throssell, J. Montgomery, J. Peralta, F. Ogliaro, M. Bearpark, J. Heyd, E. Brothers, K. Kudin, V. Staroverov, T. Keith, R. Kobayashi, J. Normand, K. Raghavachari, A. Rendell, J. Burant, S. Iyengar, J. Tomasi, M. Cossi, J. Millam, M. Klene, C. Adamo, R. Cammi, J. Ochterski, R. Martin, K. Morokuma, O. Farkas, J. Foresman and D. J. Fox, *Gaussian 16 revision B.01*, Gaussian Inc., Wallingford, CT, 2016.
52 F. Santoro, R. Improta, A. Lami, J. Bloino and V. Barone, *J. Chem. Phys.*, 2007, **126**, 84509.
53 F. Santoro, A. Lami, R. Improta and V. Barone, *J. Chem. Phys.*, 2007, **126**, 184102.
54 J. von Cosel, J. Cerezo, D. Kern-Michler, C. Neumann, L. J. G. W. van Wilderen, J. Bredenbeck, F. Santoro and I. Burghardt, *J. Chem. Phys.*, 2017, **147**, 164116.
55 Q. Cao, X. Guan, M. W. George, D. L. Phillips, C. Ma, W. M. Kwok, M. Li, Y. Du, X.-Z. Sun and J. Xue, *Faraday Discuss.*, 2010, **145**, 171.
56 H. Bian, J. Li, X. Wen, Z. Sun, J. Song, W. Zhuang and J. Zheng, *J. Phys. Chem. A*, 2011, **115**, 3357.
57 L. Whaley-Mayda, A. Guha, S. B. Penwell and A. Tokmakoff, *J. Am. Chem. Soc.*, 2021, **143**, 3060.
58 D. Warther, S. Gug, A. Specht, F. Bolze, J.-F. Nicoud, A. Mourot and M. Goeldner, *Bioorg. Med. Chem.*, 2010, **18**, 7753.